NOAA Technical Report NESS 76

Determination of the Earth-Atmosphere Radiation Budget From NOAA Satellite Data

Washington, D.C.
November 1977

U.S. DEPARTMENT OF COMMERCE
National Oceanic and Atmospheric Administration
National Environmental Satellite Service

NOAA TECHNICAL

National Environmental Satelli .ice Series

The National Environmental Satellite Service (NESS) is responsible for the establishment and operation of the environmental satellite systems of NOAA.

Publication of a report in NOAA Technical Report NESS series will not preclude later publication in an expanded or modified form in scientific journals. NESS series of NOAA Technical Reports is a continuation of, and retains the consecutive numbering sequence of, the former series, ESSA Technical Report National Environmental Satellite Center (NESC), and of the earlier series, Weather Bureau Meteorological Satellite Laboratory (MSL) Report. Reports 1 through 39 are listed in publication NESC 56 of this series.

Reports 1 through 50 in the series are available from the National Technical Information Service (NTIS), U.S. Department of Commerce, Sills Bldg., 5285 Port Royal Road, Springfield, Va. 22151, in paper copy or microfiche form. Order by accession number, when given, in parentheses. Beginning with 51, printed copies of the reports are available through the Superintendent of Documents, U.S. Government Printing Office, Washington, D.C. 20402; microfiche available from NTIS (use accession number when available). Prices given on request from the Superintendent of Documents or NTIS.

ESSA Technical Reports

NESC 43 Atlas of World Maps of Long-Wave Radiation and Albedo--for Seasons and Months Based on Measurements From TIROS IV and TIROS VII. J. S. Winston and V. Ray Taylor, September 1967, 32 pp. (PB-176-569)

NESC 44 Processing and Display Experiments Using Digitized ATS-1 Spin Scan Camera Data. M. B. Whitney, R. C. Doolittle, and B. Goddard, April 1968, 60 pp. (PB-178-424)

NESC 45 The Nature of Intermediate-Scale Cloud Spirals. Linwood F. Whitney, Jr., and Leroy D. Herman, May 1968, 69 pp. plus appendixes A and B. (AD-673-681)

NESC 46 Monthly and Seasonal Mean Global Charts of Brightness From ESSA 3 and ESSA 5 Digitized Pictures, February 1967-February 1968. V. Ray Taylor and Jay S. Winston, November 1968, 9 pp. plus 17 charts. (PB-180-717)

NESC 47 A Polynomial Representation of Carbon Dioxide and Water Vapor Transmission. William L. Smith, February 1969 (reprinted April 1971), 20 pp. (PB-183-296)

NESC 48 Statistical Estimation of the Atmosphere's Geopotential Height Distribution From Satellite Radiation Measurements. William L. Smith, February 1969, 29 pp. (PB-183-297)

NESC 49 Synoptic/Dynamic Diagnosis of a Developing Low-Level Cyclone and Its Satellite-Viewed Cloud Patterns. Harold J. Brodrick and E. Paul McClain, May 1969, 26 pp. (PB-184-612)

NESC 50 Estimating Maximum Wind Speed of Tropical Storms From High Resolution Infrared Data. L. F. Hubert, A. Timchalk, and S. Fritz, May 1969, 33 pp. (PB-184-611)

NESC 51 Application of Meteorological Satellite Data in Analysis and Forecasting. Ralph K. Anderson, Jerome P. Ashman, Fred Bittner, Golden R. Farr, Edward W. Ferguson, Vincent J. Oliver, Arthur H. Smith, James F. W. Purdom, and Rance W. Skidmore, March 1974 (reprint and revision of NESC 51, September 1969, and inclusion of Supplement, November 1971, and Supplement 2, March 1973), pp. 1--6C-18 plus references.

NESC 52 Data Reduction Processes for Spinning Flat-Plate Satellite-Borne Radiometers. Torrence H. MacDonald, July 1970, 37 pp. (COM-71-00132)

NESC 53 Archiving and Climatological Applications of Meteorological Satellite Data. John A. Leese, Arthur L. Booth, and Frederick A. Godshall, July 1970, pp. 1-1--5-8 plus references and appendixes A through D. (COM-71-00076)

NESC 54 Estimating Cloud Amount and Height From Satellite Infrared Radiation Data. P. Krishna Rao, July 1970, 11 pp. (PB-194-685)

NESC 56 Time-Longitude Sections of Tropical Cloudiness (December 1966-November 1967). J. M. Wallace, July 1970, 37 pp. (COM-71-00131)

(Continued on inside back cover)

NOAA Technical Report NESS 76

Determination of the Earth-Atmosphere Radiation Budget From NOAA Satellite Data

Arnold Gruber

Meteorological Satellite Laboratory

Washington, D.C.
November 1977

U.S. DEPARTMENT OF COMMERCE
Juanita M. Kreps, Secretary

National Oceanic and Atmospheric Administration
Richard A. Frank, Administrator

National Environmental Satellite Service
David S. Johnson, Director

CONTENTS

DETERMINATION OF THE EARTH-ATMOSPHERE RADIATION BUDGET FROM NOAA SATELLITE DATA

Arnold Gruber

Meteorological Satellite Laboratory
National Environmental Satellite Service, NOAA
Washington, D.C.

ABSTRACT. The Earth-atmosphere radiation budget has been calculated using observations obtained by the two-channel scanning radiometer aboard the NOAA operational satellites. The two channels observed reflected radiation in the visible range (0.5 to 0.7 μm) and emitted longwave radiation in the atmospheric window (10.5 to 12.5 μm). Calculations of the Earth-atmosphere radiation balance have been made since June 1974 and are continuing.

This report describes the methods and approximations used in estimating the radiation budget from the operational data. Results are presented for the annual period June 1974 through May 1975. Emphasis has been placed on the broad spatial and temporally averaged results, such as mean monthly zonal and global averages and annual maps of the radiation balance parameters, i.e., albedo, outgoing longwave radiation, absorbed radiation, and net radiation.

The global albedo was calculated as 32.3% and the outgoing longwave radiation as 248 $W \cdot m^{-2}$.

INTRODUCTION

The distribution of the net radiation of the Earth-atmosphere system is of fundamental importance to the physics of the atmosphere and oceans over wide ranges of time and space. The net radiation of the Earth-atmosphere system is defined by

$$Q = I_0 (1-A) - E$$

where

Q = net radiation

I_0 = Incoming solar radiation

A = The Earth-atmosphere albedo

E = The outgoing thermally emitted radiation for the Earth-atmosphere system.

This report is concerned with the determination of the components of the Earth-atmosphere radiation budget from measurements made by the visible channel (0.5-0.7 μm) and infrared channel (10.5-12.5 μm) scanning radiometer aboard the NOAA satellites. Radiation budget calculations have been made on a continuing basis since June 1974. The purpose of this report is to give details of methods and approximations used in deriving the radiation budget values and to present some broad spatially and temporally averaged results.

BASIC MEASUREMENTS, UNITS, AND CALIBRATION

The measuring instrument is a scanning radiometer flown aboard a polar orbiting satellite. A description of the NOAA satellite system, including the various instruments, is provided by Schwalb (1972). The spacecraft has a 2100 local time northbound Equator crossing and a 0900 local time southbound Equator crossing. The radiometer senses reflected energy in the visible spectrum 0.5 to 0.7 μm and emitted energy in the 10.5 to 12.5 μm infrared window.

The resolution of the visible channel is 4 km at the satellite subpoint and for the infrared channel it is 8 km at the subpoint. The infrared channel has an onboard calibration system; the visible channel does not. However, it has been possible to calibrate the visible channel using laboratory data (Appendix 1). The laboratory calibration has been verified by an inflight calibration using an Earth target (Jacobowitz and Gruber 1975). The calibration of the data is discussed in more detail by Conlan (1973).

In the infrared part of the spectrum (10.5 to 12.5 μm), the calibrated signal is expressed as equivalent blackbody temperatures through use of the Planck equation. The temperatures are in turn expressed in coded digital values from 0 to 255 corresponding to a temperature range 164 K to 310 K (see table 3, Conlan 1973).

The calibrated visible channel data are also expressed in coded values of 0 to 255. However, in this case the digital values represent reflected energy expressed in foot-lamberts, with a range of 0 to 10,099 (table 2, Conlan 1973). Foot-lamberts, however, are not suitable units for use in reflected energy. They have to be converted to appropriate energy units by first determining the luminous efficiency (lumens/Watt) of the system. Such a determination for NOAA 2 is shown in Appendix 1. The same procedure was performed for NOAA 3 and 4.

Prior to Sept. 15, 1976, the coded values of data were archived on a square 2048 x 2048 grid per hemisphere. Since that time the data have been archived on a 1024 x 1024 grid which is alined with the NMC polar stereographic grid. In an attempt to normalize the visible data to an overhead Sun, each observation is multiplied by Sec Z, where Z is the solar zenith angle. A limb darkening correction is applied to the IR data when they are not in the nadir mode. The correction is empirical and depends upon the viewing angle and observed equivalent blackbody temperature. Implicit in this procedure is a correction for increased water vapor in the slant path over the water vapor content in the column when looking straight down.

DETERMINATION OF ALBEDO FROM VISIBLE CHANNEL RADIANCE

The geometry of the reflection of energy is shown in figure 1, adopted from Ruff, et al. (1967). A spherical coordinate system is centered at the point of reflection, having coordinates of satellite zenith angle, θ, and of azimuth, α. The azimuth is relative to the azimuth of the solar beam and is positive in a clockwise direction.

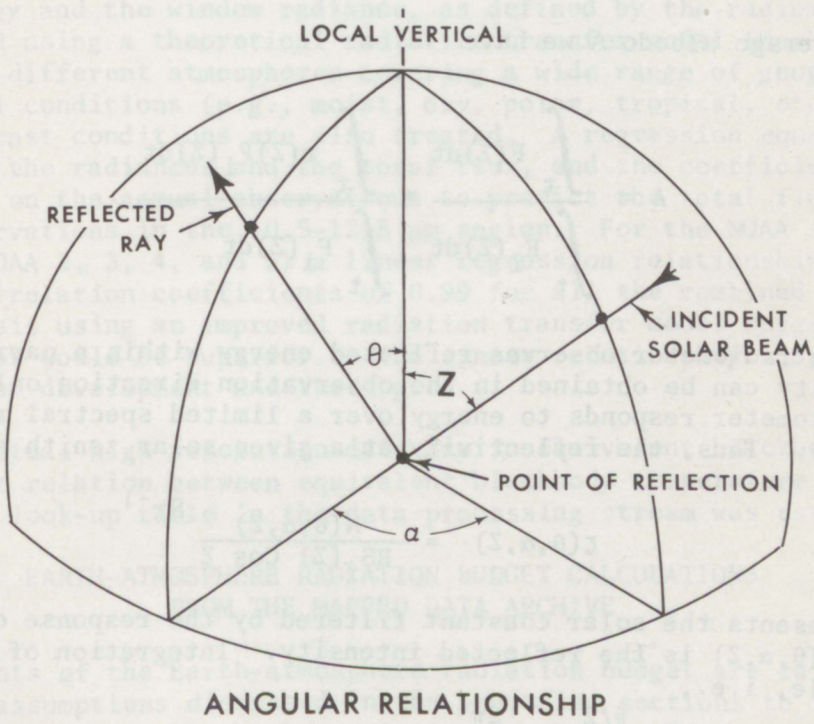

Figure 1.--Diagram of upward-facing unit hemisphere, showing reflection geometry.

If $I(\theta,\alpha,Z)$ is the reflected intensity ($W \cdot m^{-2} \cdot S_r^{-1}$) at zenith angle θ, azimuth angle α, and solar zenith angle Z, the flux density from a unit horizontal is

$$F(Z) = \int_0^{\pi/2} \int_0^{2\pi} I(\theta,\alpha,Z) \, \mathrm{Sin}\, \theta \, \mathrm{Cos}\, \theta \, d\alpha d\theta \qquad (1)$$

The flux incident on a horizontal surface is given by

$$F_i(Z) = R \, S_0 \, \mathrm{Cos}\, Z \qquad (2)$$

where S_0 is the solar constant and R weights the solar constant according to departures from the mean Earth-Sun distance;

$$R = \frac{\bar{d}^2}{d^2}$$

where $\bar{d}$ is the mean Earth-Sun distance and d is the actual Earth-Sun distance at a given time.

The albedo at any given instant of time is defined as the ratio of 1 to 2, i.e.,

$$r(Z) = \frac{F(Z)}{F_i(Z)} . \tag{3}$$

For a daily average albedo A we have

$$A = \frac{\int_t F(Z)dt}{\int_t F_i(Z)dt} = \frac{\int_t r(Z)F_i(Z)dt}{\int_t F_i(Z)dt} . \tag{4}$$

The scanning radiometer observes reflected energy within a narrow field and the reflectivity can be obtained in the observation direction only. Furthermore, the radiometer responds to energy over a limited spectral region (about 0.5 to 0.7 μm). Thus, the reflectivity at a given solar zenith angle can be expressed as

$$\zeta(\theta,\alpha,Z) = \frac{N(\theta,\alpha,Z)}{RS_f(Z)\ \mathrm{Cos}\ Z}\ \mathrm{Sr}^{-1} \tag{5}$$

where S_f represents the solar constant filtered by the response of the radiometer and $N(\theta,\alpha,Z)$ is the reflected intensity. Integration of eq (5) over the solid angle, i.e.,

$$\int_0^{\pi/2}\int_0^{2\pi} \zeta(\theta,\alpha,Z)\ \mathrm{Cos}\ \theta\ \mathrm{Sin}\ \theta\ d\alpha d\theta, \tag{6}$$

provides a measure of A(Z) provided that it is assumed that the reflectance calculated by eq (6) using filtered data is identical to the reflectance calculated using unfiltered radiances.

To solve eq (6) for the reflectance, it is necessary to know $\zeta(\theta,\alpha,Z)$ as a function of θ and α. In general, this dependence is unknown, although various investigators have attempted to model this dependence, based on limited samples of observations (e.g., Raschke et al. 1973a, b; Ruff et al. 1967). Since well-defined angular models are not yet available, isotropy was assumed. Thus $\zeta(\theta,\alpha,Z) = \zeta(Z)$, i.e., ζ is not dependent on θ and α, and the reflectance is simply given as $r(Z) = \pi\zeta(Z)$. If we further assume that r is not dependent on Z, then r is a measure of the average daily albedo of the Earth-atmosphere system as shown in eq (4).

DETERMINATION OF FLUX OF OUTGOING LONGWAVE RADIATION FROM INFRARED WINDOW RADIANCE

The determination of the flux of outgoing longwave radiation in the spectral interval of about 4-50 μm from radiance measurements in the window region (10.5-12.5 μm) is treated differently than in the case of reflected energy. The procedure is to correlate the window radiance corrected for limb darkening, as previously mentioned, to the outgoing flux. Both the total flux of longwave energy and the window radiance, as defined by the radiometer response, are calculated using a theoretical radiative transfer model (Wark, et al. 1962) applied to 99 different atmospheres covering a wide range of geographical and meteorological conditions (e.g., moist, dry, polar, tropical, etc.). Cloud-free and overcast conditions are also treated. A regression equation is calculated between the radiances and the total flux, and the coefficients derived are then used on the actual observations to predict the total flux from the radiance observations in the 10.5-12.5 μm region. For the NOAA series of satellites (NOAA 2, 3, 4, and 5) a linear regression relationship was calculated with correlation coefficients of 0.99 for all the combined cases. Subsequent analysis using an improved radiation transfer model suggests that a curvilinear fit would be superior to the linear relationship. Such a fit is currently under development and testing.

Since the actual high-resolution data are in equivalent blackbody temperature, a direct relation between equivalent blackbody temperature and flux in the form of a look-up table in the data processing stream was established.

EARTH-ATMOSPHERE RADIATION BUDGET CALCULATIONS FROM THE MAPPED DATA ARCHIVE

The components of the Earth-atmosphere radiation budget are calculated by applying the assumptions discussed in the preceding sections to the mapped data archive. However, the high resolution of that archive represents an enormous amount of data and poses a significant storage and retrieval effort for the development of continuous data sets. Furthermore, primary interest is in radiation budget parameters over the globe on scales of about 150-250 km. This scale is consistent with general circulation models and is the preferred scale for diagnostic studies of the 15 day-5 yr climatic fluctuations. Consequently, the radiation budget values were obtained by averaging 16 x 16 subsets of this high-resolution data and forming a reduced array (125 x 125) alined with the NMC polar stereographic map base. This array is designated as the polar archive. This was done for both the outgoing longwave radiation and the reflected energy, although, as discussed later, those fields are treated differently further downstream in the processing. Besides reducing the size of the data processing effort, averaging 16 x 16 subsets of the data also reduces the random errors. Any average composed of less than one-half the maximum number of data points was considered as a missing observation in the polar archive. Noisy and other erroneous data, which may appear as valid digital values in the mapped archive and thus be included in the averages, are easily identified by inspection of operationally produced photographic images and are removed from the polar archive. The data calculated and archived on a daily basis are the outgoing longwave flux, both nighttime and daytime, the absorbed solar energy, and the available incoming solar energy.

We do not archive albedo since operations on the space and time domain (averaging and interpolating) require weighting by the incoming solar energy (see Appendix 2). Since that is not the case for the absorbed and incoming solar energy, it is computationally simpler for future operations to archive those quantities and calculate albedo when required.

The daily absorbed solar energy is calculated by first estimating the reflectance using the calibration procedures given in Appendix 1 and, as discussed earlier, assuming isotropy and no solar zenith angle dependence to obtain an estimate of the daily albedo. The daily incoming solar energy for a given location is readily calculated using an assumed solar constant* of 1353 $W \cdot m^{-2}$. The absorbed solar energy is given as SI_0 (1-A), where S is the absorbed solar energy, A is the albedo, and I_0 is the incoming solar energy.

As shown in Appendix 1, the relationship between digital counts and reflected energy is linear, so that digital counts are averaged to obtain estimates of reflected energy at low resolution. However, this is not the case for the outgoing longwave energy, which requires that each high-resolution data point be converted to a flux value prior to averaging.

The radiation budget components in the polar stereographic archive (except for available solar energy) are also archived on a global 2 1/2° latitude by 2 1/2° longitude array using a bilinear interpolating procedure to transfer from the polar archive to the fixed latitude longitude array. Such an array is useful for mapping the data onto a mercator map projection and producing zonal mean values. The bilinear interpolation is restricted to the immediate four data points surrounding the latitude-longitude intersection. Should any of those data points be missing, no interpolation is performed and that latitude longitude intersection is considered missing. After all possible grid values are obtained, a two-dimensional interpolating procedure is used to fill in the missing values. Days with more than 50% of the maximum possible data points missing are considered missing days.† When interpolating for reflected solar energy, ‡ the polar night latitude is used as a zero-boundary condition in the interpolation routine. The interpolated field is not allowed to yield physically unrealistic values by constraining the interpolated values to be less than the incoming solar energy. If an interpolated value should exceed the incoming solar energy it is constrained to 0.95 (I_0). This situation is most likely to occur when there are large data gaps, such as during the Southern Hemisphere winter when the satellite viewing and Sun

---

*The value 1353 $W \cdot m^{-2}$ is chosen for this computation based on the report by Thekaekara and Drummond (1971). However, the Earth Radiation Budget (ERB) experiment on NIMBUS 6 measured 1392 $W \cdot m^{-2}$. In sections of the report where values of albedo, net radiation, and absorbed solar radiation are presented, we scaled the values to 1392 $W \cdot m^{-2}$. This was done to facilitate comparisons with the ERB.

†Because of the polar night, the maximum possible number of data points for reflected energy is generally less than the 72 x 144, 2 1/2° latitude-longitude points that cover the globe.

‡ Interpolations are performed on reflected solar energy, but absorbed solar energy is archived.

geometry result in large data-void regions extending equatorward of the polar night latitudes. This requires extensive interpolation.

The 2 1/2° latitude-longitude fields, denoted as the "Mercator" archive, serve as the primary source for future calculations of the radiation budget parameters. From it are produced mean monthly and seasonal Mercator maps (60°N-60°S) as well as zonal, hemispherical, and global averages. The polar stereographic archive serves as a backup to the Mercator archive as well as the source of data for polar stereographic maps of heat budget quantities from 50° latitude to the Poles. From the four separate fields archived on a daily basis--daytime and nighttime flux of outgoing longwave radiation, absorbed solar energy, and available solar energy--other fields are computed, averaged, and mapped. They are albedo, net radiation, average of day and night longwave flux, and difference between day and night longwave flux. However, those fields are not archived.

DATA QUALITY

Since the data used to estimate albedo and outgoing longwave radiation do not represent the best spectral interval within which to measure those fields, and since many simplifying assumptions are made in arriving at an estimate of the albedo and outgoing longwave radiation, there is some question concerning the quality of these data as estimates of radiation balance components. This situation is further compounded by the existence of small but systematic noise characteristics of the system (Leese 1977) and the lack of onboard calibration for the visible radiometer.

Therefore, assessment of the quality is not straightforward. It is known that, for individual locations and for certain kinds of surfaces, the assumptions made were so restrictive that the data may not be useful. For example, over a cloud-free water surface, areas of sunglint yield relatively high albedo when in fact the albedo should be low. When dealing with individual locations on a daily basis this situation can lead to erroneous results. Conversely, large space and time averages tend to smooth these effects and yield what appears to be representative values of albedo. This is suggested by a comparison of mean monthly wide angle measurements made by the Earth Radiation Budget (ERB) instrument on Nimbus 6 with these results for the period July 1975 to January 1976. The wide-angle ERB (Smith et al. 1977) is an experiment designed to measure Earth radiation budget parameters on a global scale using observations of the full Earth's disk. It does not suffer from the deficiencies of an instrument sampling a narrow field of view, which can be quite difficult to overcome. Also, ERB takes measurements over the spectral interval 0.3-5.0 μm, and so covers the full range of reflected energy. Although ERB suffers some deficiencies in sampling and data reduction, it should provide a highly representative, independent estimate of Earth-atmosphere albedo. The comparison between these two sets of observations from July 1975-January 1976 is shown in figure 2. The albedo calculated from the scanning radiometer data was adjusted to a solar constant of 1392 $W \cdot m^{-2}$, the value measured by ERB.

It should be noted that there is approximately a 3-hr difference in observing time and that the ERB measurements are preliminary and still subject to further investigation by the ERB research team. The agreement in albedo is

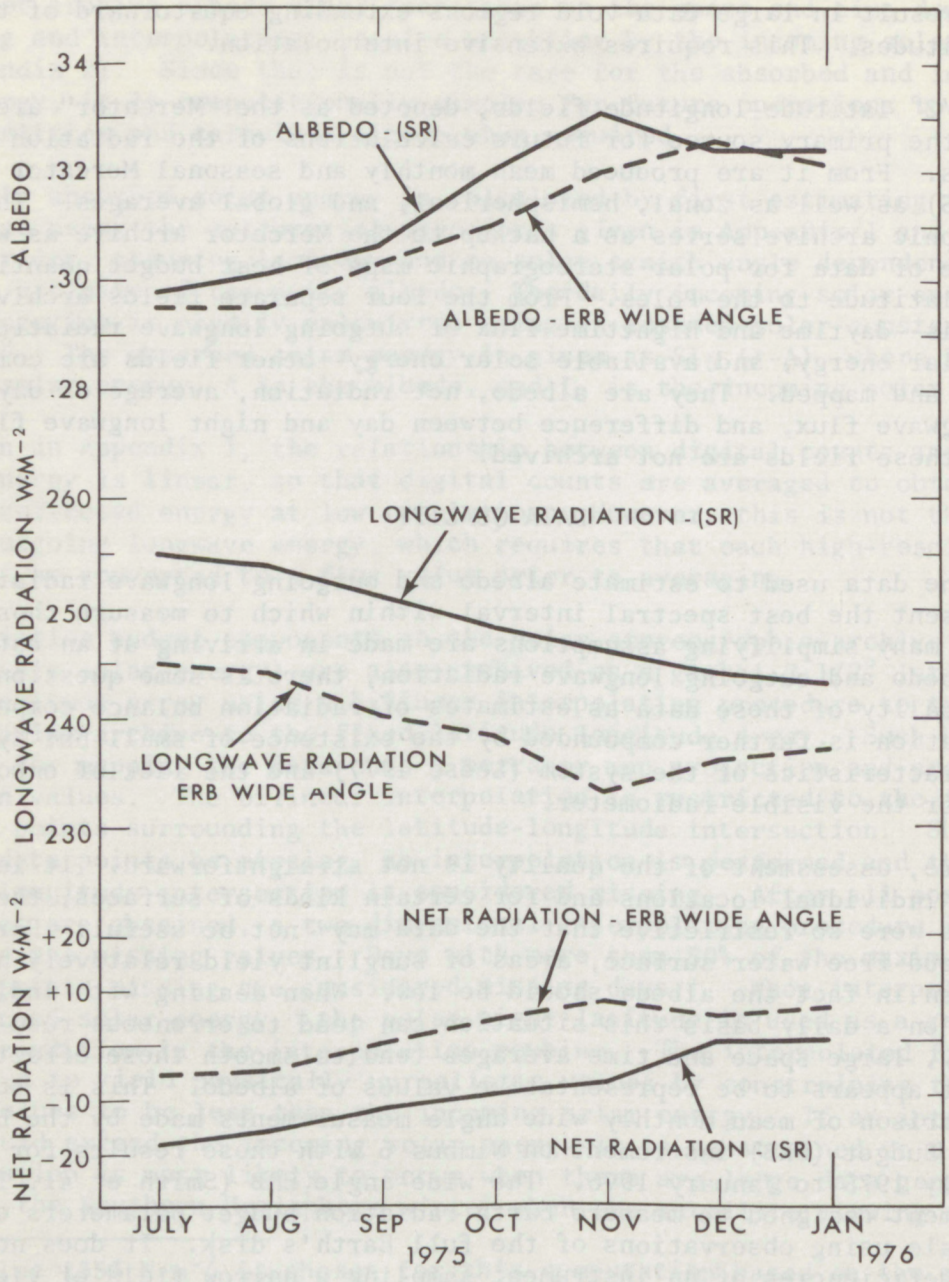

Figure 2.--Comparison of albedo, outgoing longwave radiation, and net radiation observations between the operational NOAA Scanning Radiometer data and the Earth Radiation Budget (ERB) wide-angle observations. (After Gruber 1976).

seen to be reasonably close, the largest difference being about 1%, with the best agreement in December 1975 and January 1976. The good agreement in those months is somewhat misleading because a systematic drop in albedo, apparently due to instrument degradation on NOAA 4, was noted starting in December 1975 and continued until NOAA 5 became operational in September 1976. Appendix 3 presents evidence detailing the nature of the systematic error. The point to be stressed is that the large-scale time averaged data appears to give reasonable values of albedo despite the simplifying assumptions, and discounting the apparent instrument degradation. This is consistent with some preliminary results of Ruff et al. (1967) in their comparison of angularly corrected albedo with albedo calculated assuming isotropy. They found only a slight difference in the profile of zonally averaged albedo between the two.

The comparison of outgoing longwave flux shows what appears to be a systematic difference of about 10 $W \cdot m^{-2}$ between the ERB values and these results. There is no readily available explanation for this difference, although the limb darkening corrections and the regression models currently employed are prime suspects. Work is now in progress examining both these aspects by recalculating the window radiance using updated transmission functions in the model development.

RESULTS

This section will concentrate on monthly seasonal and annual characteristics of the net radiation and its principal components for the period June 1974 through May 1975, the first full year of processed data. Attention is being focused on this period, rather than the entire data set, because of the apparent systematic errors in albedo as detailed in Appendix 3.

The annual cycles in the global radiation parameters based on a 1-yr data sample of monthly means from June 1974 through May 1975 are shown in figure 3. The maximum and minimum albedos occur during the northern winter and summer months, respectively. The outgoing longwave radiation is generally out of phase with the albedo, the maximum occurring during the summer months and the minimum during the winter. The out-of-phase relationship is due primarily to the influence of cloudiness which is the principal modulator of both the reflected and outgoing longwave radiation. The absorbed radiation has a small variation during the course of the year. Consequently, the net radiation exhibits a variation determined mainly by the outgoing longwave radiation. Except for the absorbed solar energy these distributions are consistent with other estimates of the annual cycles as determined from satellite data (Jacobowitz et al. 1977, Ellis and VonderHaar 1976). The other estimates show a more pronounced cycle of absorbed solar energy than do these data. Too much significance should not be attached to the negative values of net radiation shown in figure 3 and the globally averaged values ($-12\ W \cdot m^{-2}$) shown in table 1, as the net radiation is the small difference between large quantities. Furthermore, the possibility of an incorrect limb darkening correction on the operational data and in the fluxes used in the regression model, as previously mentioned in the comparison with ERB results, can account for most of the discrepancy. If the global annual average of net radiation ($-12\ W \cdot m^{-2}$) were removed from the annual cycle, the Earth-atmosphere system would show a surplus from November through April and a deficit from May through October.

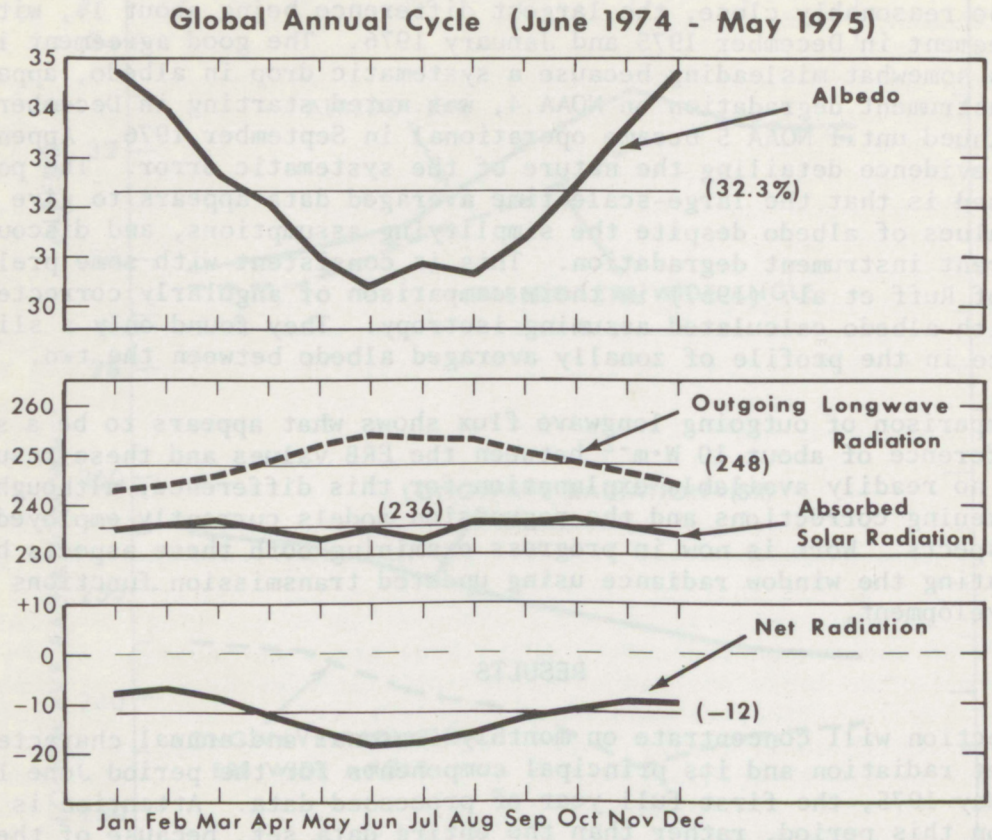

Figure 3.--The annual cycle of global averages of albedo (%), outgoing longwave radiation, absorbed solar radiation, and net radiation ($W \cdot m^{-2}$) estimated from the operational data. The averages are based on 1 yr of data, June 1974 through May 1975.

Table 1.--Global annual averages of the radiation balance parameter*,†

Outgoing longwave radiation	248 $W \cdot m^{-2}$
Albedo	32.3%
Absorbed	236 $W \cdot m^{-2}$
Net	-12 $W \cdot m^{-2}$

*Based on 1 yr of data, June 1974 through May 1975
†Solar constant = 1392 $W \cdot m^{-2}$

The estimate of global annual average albedo of 32.3% is higher than previous satellite estimates of 29.3%* (VonderHaar and Suomi 1971) and 27.7%* (Raschke et al. 1973a, b), although it is in closer agreement with the value of 31% reported by Jacobowitz et al. (1977) using ERB data. It is difficult to assess the importance of these differences because, while they all represent satellite estimates, each satellite system was different in its instrumentation, orbital characteristics, and spatial resolution, and required different assumptions and approximations in arriving at estimates of heat budget parameters. Furthermore, none of the shortwave measurements were calibrated on board the satellite. Thus, most of the differences may be due to the observing systems rather than real Earth-atmosphere behavior.

The radiation balance components undergo significant variations at most latitudes during the course of an annual cycle. This is shown in figure 4, which presents meridional profiles of net radiation for the four seasons (Northern Hemisphere): winter (Dec., Jan., Feb.), spring (Mar., Apr., May), summer (Jun., Jul., Aug.), and fall (Sep., Oct., Nov.). The tropical belt between about 10N and 10S exhibits a net radiation surplus throughout the year. Each hemisphere shows its primary surplus during its summer season. An interesting feature is the lack of symmetry between the north-south gradients in each hemisphere during the spring and summer seasons. During the Southern Hemisphere spring season the north-south gradient of net heating is small between the Equator and 30S, while in the Northern Hemisphere spring the net radiation is somewhat higher in the 0-10N latitude belt and the north-south gradient is considerably larger (about a factor of 2) than its Southern Hemisphere counterpart between latitudes 10-30. Also, the Southern Hemisphere summer exhibits considerably more surplus of net radiation in the latitude range of 10-40S as compared to its Northern Hemisphere counterpart. These characteristics are similar to the observations of VonderHaar and Suomi (1971), who studied 39 months of satellite data between the years of 1962 and 1966, although they calculated greater surpluses and smaller deficits than these data indicate.

An important thing to learn from the distribution of net heating surpluses and deficits with latitude are the meridional energy transports by the Earth-atmosphere system required for energy balance. The required meridional transport of energy for annual mean conditions has been made assuming no net heating (this required removal of the net radiation imbalance previously mentioned). The results are shown in figure 5 along with estimates made using other satellite data for comparison. In the Northern Hemisphere there is good agreement with the results of VonderHaar and Suomi (1971), and Oort and VonderHaar (1976); but appreciably less transport than Raschke et al. (1973) calculated using Nimbus 3 data. In the Southern Hemisphere these results indicate greater poleward transport than previous estimates. The assumptions made in deriving these estimates obviously limit confidence in the absolute values of the meridional transports. However, the point to be made is that these estimates are in essential agreement with other previously derived estimates, and in terms of year-to-year differences have the potential of being quite useful in the diagnosis of the large-scale circulation since systematic errors will cancel.

---

*Scaled to a solar constant of 1392 $W \cdot m^{-2}$ for purposes of comparison.

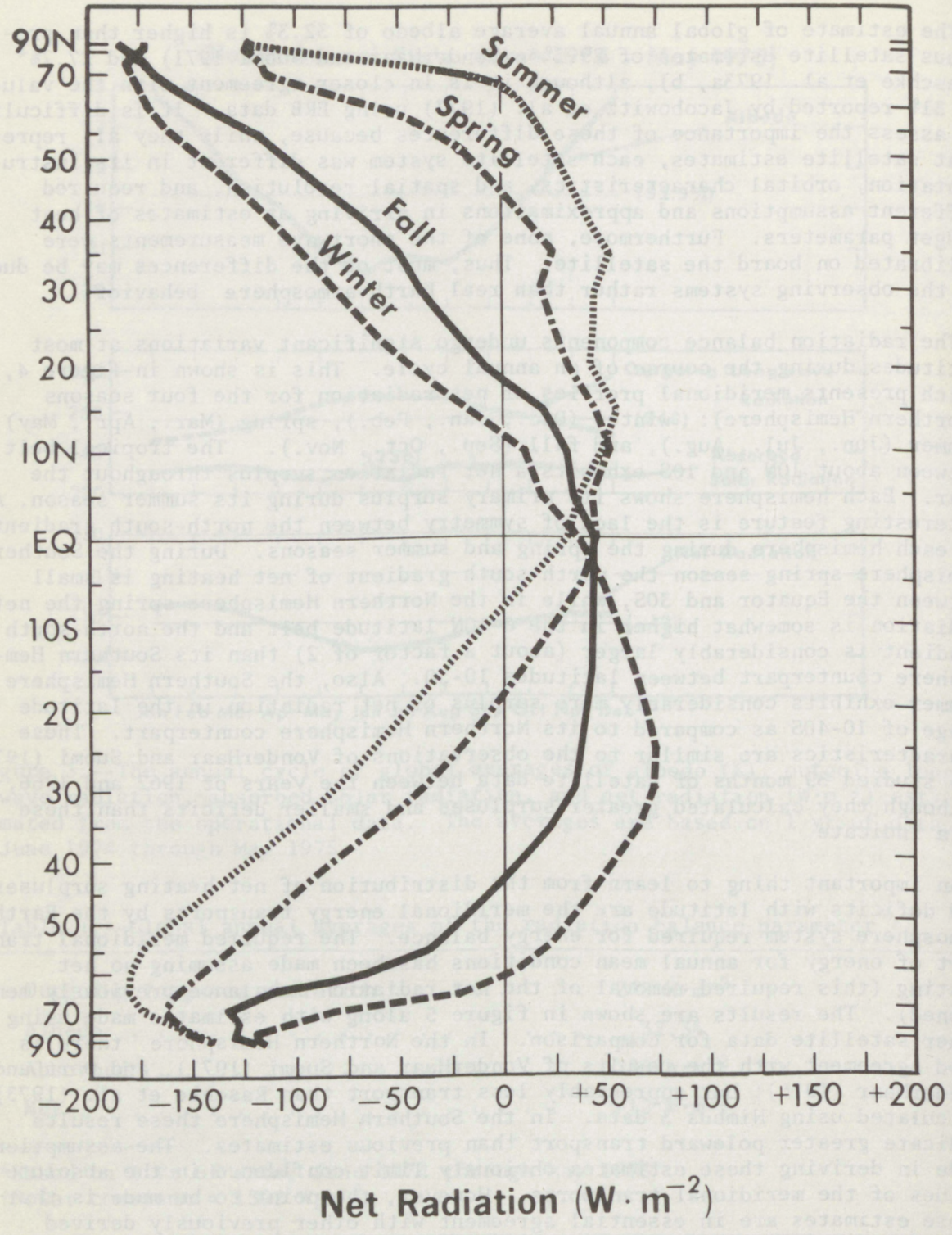

Figure 4.--Profiles of net radiation for the summer (June, July, August), fall (September, October, November), winter (December, January, February), and spring (March, April, May) seasons. Based on 1 yr of data, June 1974 through May 1975.

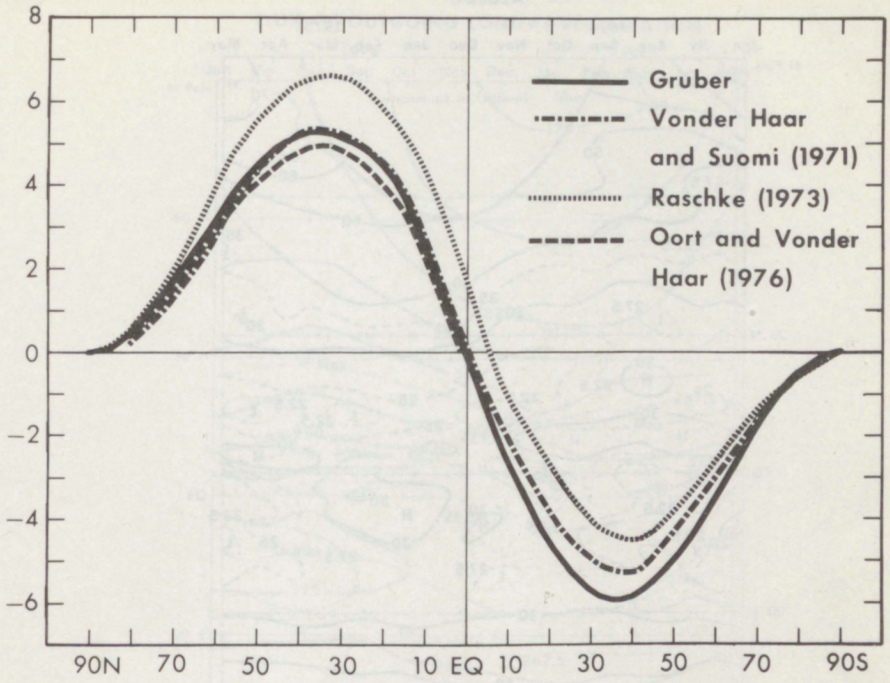

Figure 5.--Mean annual meridional transport (10^{15} Watts) based on data shown in figure 4. Positive values are northward transport and negative values are southward transport.

Further details about the temporal variation of the radiation balance components are shown in figures 6, 7, 8, and 9, which show the time-latitude distribution of zonally averaged monthly mean albedo, outgoing longwave radiation flux, absorbed solar radiation, and net radiation for the period June 1974 through May 1975. The major features of the annual course of albedo are qualitatively similar to an earlier study by Winston (1971), who examined an entire year of ESSA 3 and 5 brightness data, and the temporally limited study by Raschke et al. (1973a), who studied Nimbus 3 radiation data. They are similar to the results of Jacobowitz et al. (1977) who studied ERB data. Those features are higher values of albedo at higher latitude, a secondary maximum primarily north of the Equator associated with the ITCZ, and lower values in the tropics and subtropics of both hemispheres. An annual cycle in albedo is evident at most latitudes, its largest amplitude being in middle latitudes of the Northern Hemisphere. In the middle latitudes of both hemispheres the maximum albedo occurs during the winter months. In the subtropics (10°-20°N,S) the phase reverses, with a minimum in winter months and maximum during the summer months. In the belt 5-10°N (ITCZ region) an annual cycle is not so clearly evident. However, the albedo appears to reach a maximum during the June-October period. The excursion of the albedo in the ITCZ region into the Southern Hemisphere during January and February is principally a result of the southward shift of cloudiness over Africa, South America, and the Indonesian-Melanesian area. Over the open oceanic areas the cloudiness associated with the ITCZ generally remains north of the Equator (Gruber 1972).

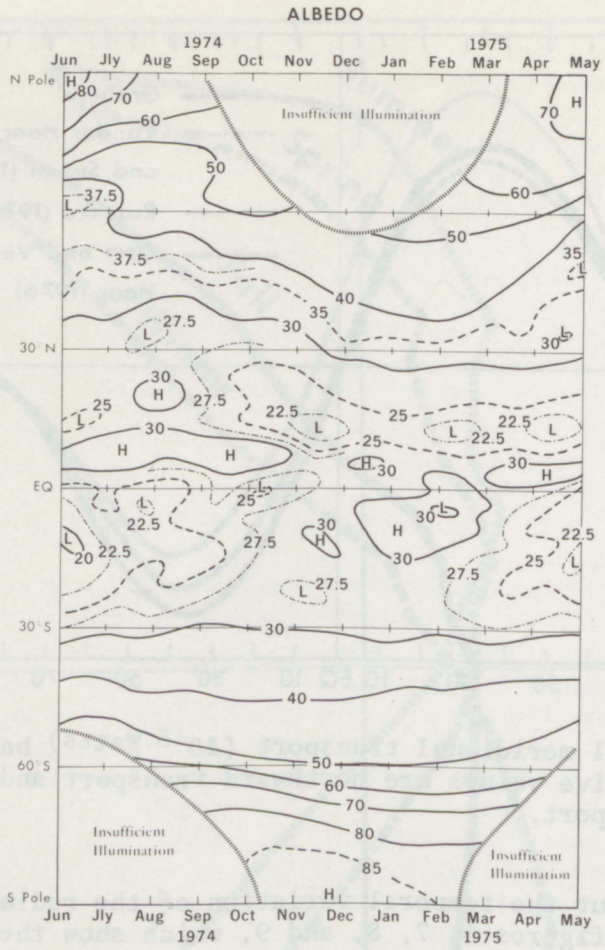

Figure 6.--Time-latitude section of mean monthly albedo in percent every 2.5° latitude for the period June 1974 through May 1975.

The outgoing longwave radiation exhibits many of the same characteristics of the albedo but in an inverse sense. This is not surprising since much of the cloudiness over the globe extends into the middle and upper troposphere giving rise to the condition of high albedo and low outgoing longwave radiation. Thus, there are lower values of outgoing longwave radiation toward the Poles, higher values of outgoing longwave radiation in the subtropical belts, and a secondary minimum in the equatorial zone, primarily north of the Equator and associated with the ITCZ. As in the case of the albedo, the annual cycle is more pronounced in the Northern Hemisphere than in the Southern Hemisphere. Maximum values occur in the middle and polar latitudes during the summer months in both hemispheres. Also, in the case of albedo, phase reversals take place in the 5°-20°N, and 0°-20°S region.

The annual variation of absorbed solar energy is shown in figure 8. Outside the 5°-10°N latitude belt (ITCZ region), a pronounced annual variation is observed with the maximum of absorbed energy occurring during the summer months of each hemisphere, regardless of latitude. The phase of the variation clearly follows the course of the Sun during the year, as seen by following

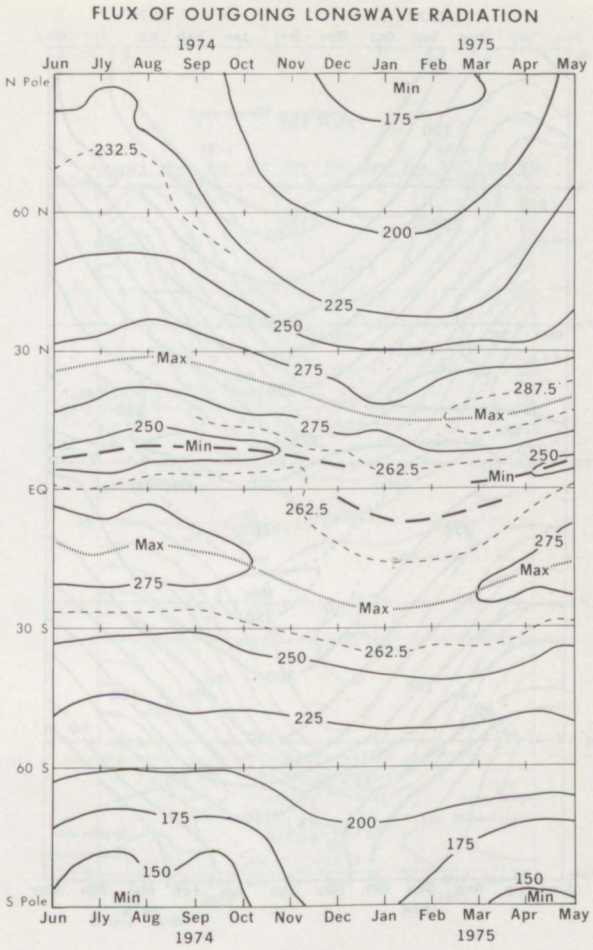

Figure 7.--Time-latitude section of mean monthly outgoing longwave radiation in $W \cdot m^{-2}$ for the period June 1974 through May 1975.

the solar declination plotted in figure 8. The reason for this variation is that the temporal variation of the incoming solar energy is much greater than the temporal variation of the albedo; thus, the phase of the absorbed solar energy is essentially determined by the temporal variation of incoming solar energy. This can be demonstrated by a simple model. Consider the incoming solar energy and the albedo as simple sinusoidal functions of time:

$$I(t) = I_m + I_0 \text{ Cos } (\omega t + \phi') \tag{7}$$

$$A(t) = A_m + A_0 \text{ Cos } (\omega t + \phi)$$

where I is the incoming solar energy, A is the albedo, ω is the annual period, and ϕ', ϕ are the phases. Subscript m represents the mean value and subscript 0 represents the amplitude of the variation. The absorbed energy as a function of time is

$$AB(t) = (1-A)I \ . \tag{8}$$

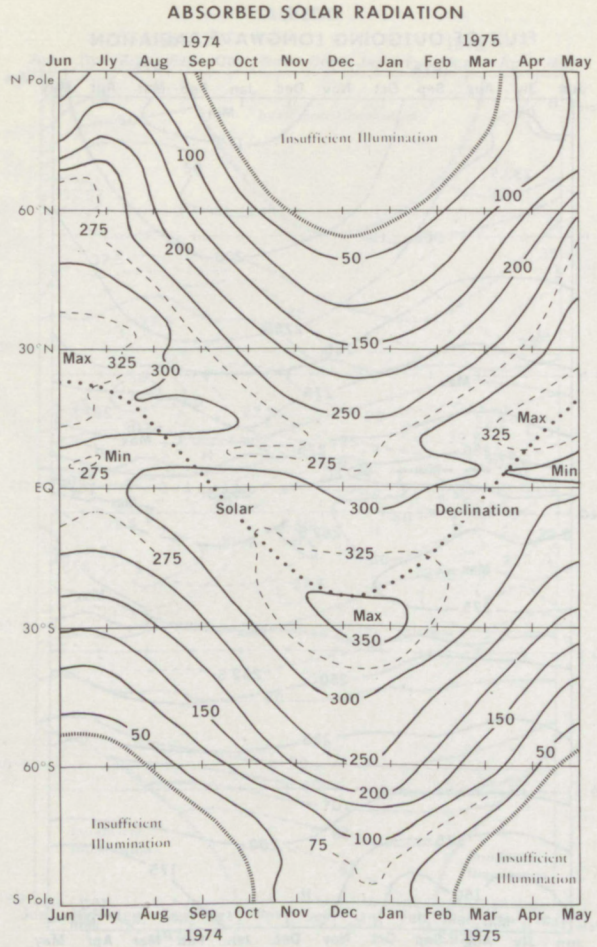

Figure 8.--Time-latitude section of mean monthly absorbed solar radiation in $W \cdot m^{-2}$ for the period June 1974 through May 1975.

Substituting from eq (1) yields

$$Ab(t) = [I_m + I_0 \text{ Cos } (\omega t + \phi)] \times [1-A_m-A_0 \text{ Cos } (\omega t + \phi')]. \quad (9)$$

A_0, the amplitude of the albedo as determined from figure 6, is generally 10% of the mean values or less and can probably be neglected. Thus $Ab(t) \simeq (I_m I_0 \text{ Cos } (\omega t + \phi)^* (1-A_m)$, and the temporal variation of absorbed energy is essentially determined by the variation of incoming solar energy scaled by $(1-A_m)$.

The net energy also exhibits a pronounced annual variation with phase relationships similar to the absorbed solar energy, i.e., maximum of net radiation during the summer months of both hemispheres. The maximum and surplus of energy also follow the solar declination. The reason for this is that the temporal variation of net radiation is dominated by the variation in absorbed solar energy, which has a much greater amplitude than the variation of outgoing longwave radiation. The exception to this, of course, is in and near the polar night latitudes where outgoing longwave radiation dominates and determines the sign and magnitude of the net radiation.

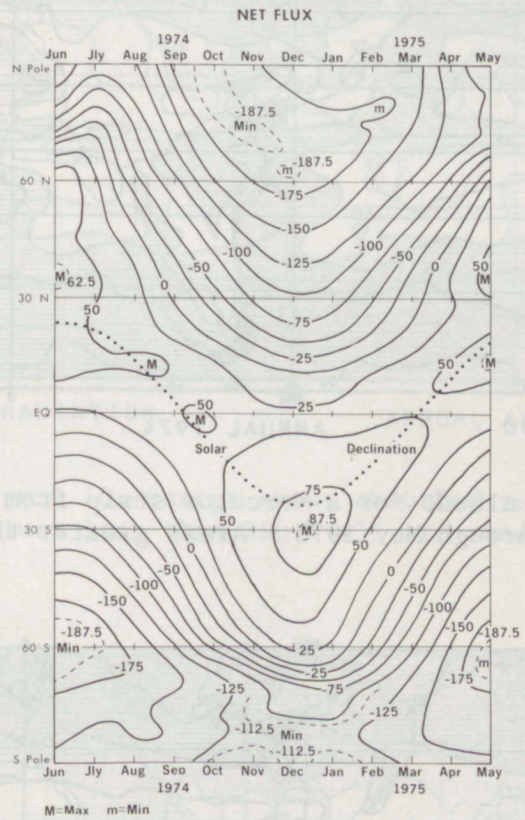

Figure 9.--Time-latitude section of mean monthly net radiation in $W \cdot m^{-2}$ for the period June 1974 through May 1975.

GEOGRAPHICAL DISTRIBUTIONS

Although Earth radiation budget estimates are calculated over fixed grid points on a daily basis, monthly averages are the shortest time period for routinely produced globally mapped outputs. Seasonal and annual maps are also routinely prepared and, as the data set extends in time, charts of year-to-year differences for months and seasons are prepared.

Preliminary studies of some of these individual months and seasons with emphasis on year-to-year differences have been made by Winston (1976) and Winston and Krueger (1977). In this report, however, emphasis is being placed on geographical variations of the annually averaged radiation budget parameters for the period June 1974 to May 1975. The annual average albedo, outgoing longwave radiation, absorbed energy, and net radiation between 60N and 60S are shown in figures 10-13. Poleward of about latitude 40N and 40S the albedo and outgoing longwave radiation show a predominantly zonal orientation, although significant perturbations do occur in the zonal direction,

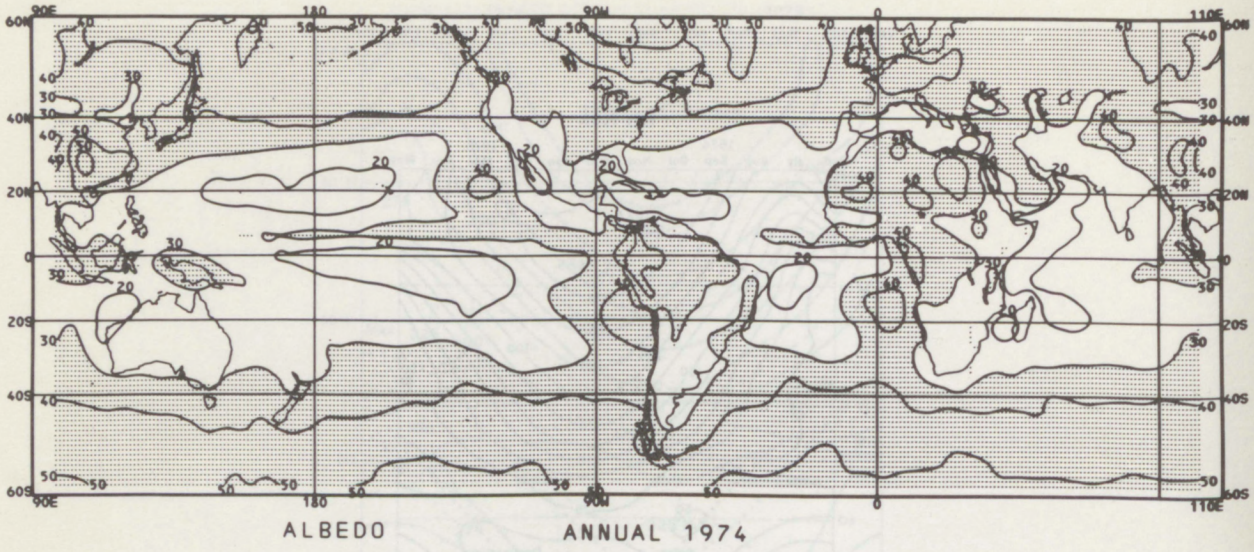

Figure 10.--Mean annual albedo for a Mercator strip from 60N to 60S based on data from June 1974 through May 1975. Areas greater than 30% are shaded.

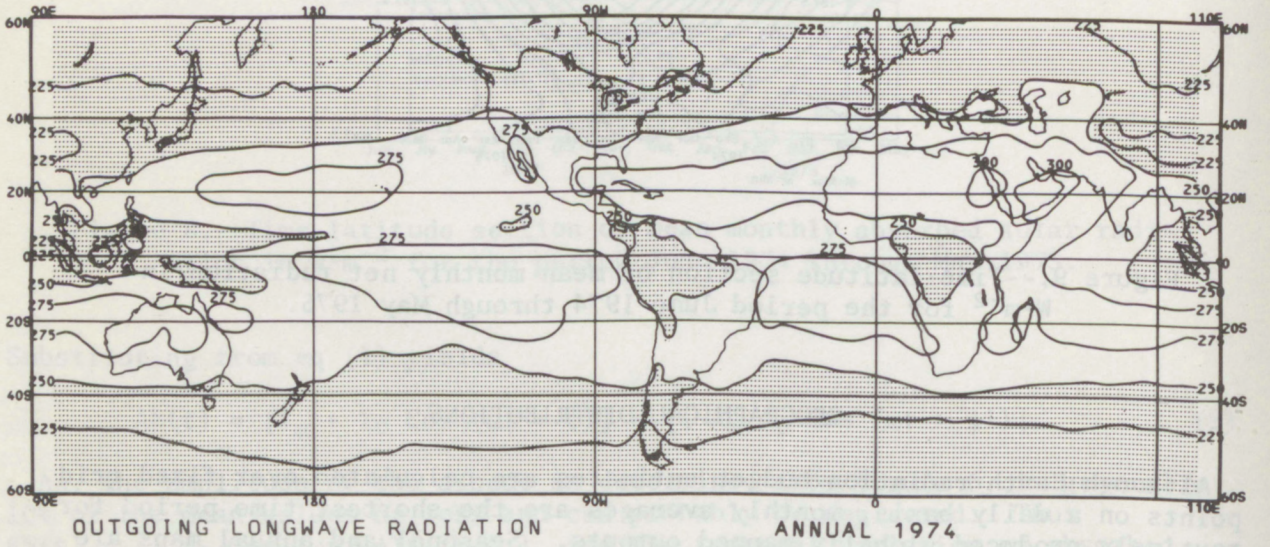

Figure 11.--Same as figure 10 except for outgoing longwave radiation. Values less than 250 $W \cdot m^{-2}$ are shaded.

particularly in the Northern Hemisphere. Towards the Equator a more pronounced east-west gradient is evident, particularly in the equatorial regions. Contributing to this east-west distribution are the major cloudiness zones over Africa, South America, and Indonesian and Western Pacific area. Those areas represent mostly deep convective and high cloudiness as indicated by the low values of outgoing longwave radiation (figure 11). Other contributions towards the variations of albedo with longitude come from the high

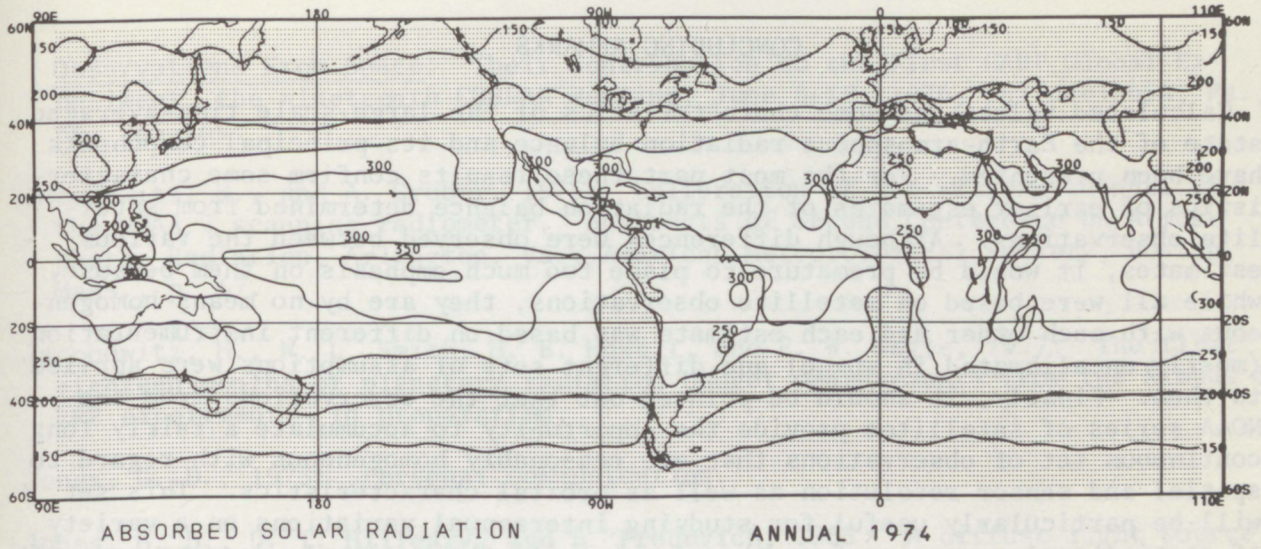

Figure 12.--Same as figure 10, except shows absorbed solar radiation ($W \cdot m^{-2}$). Values less than 250 $W \cdot m^{-2}$ are shaded.

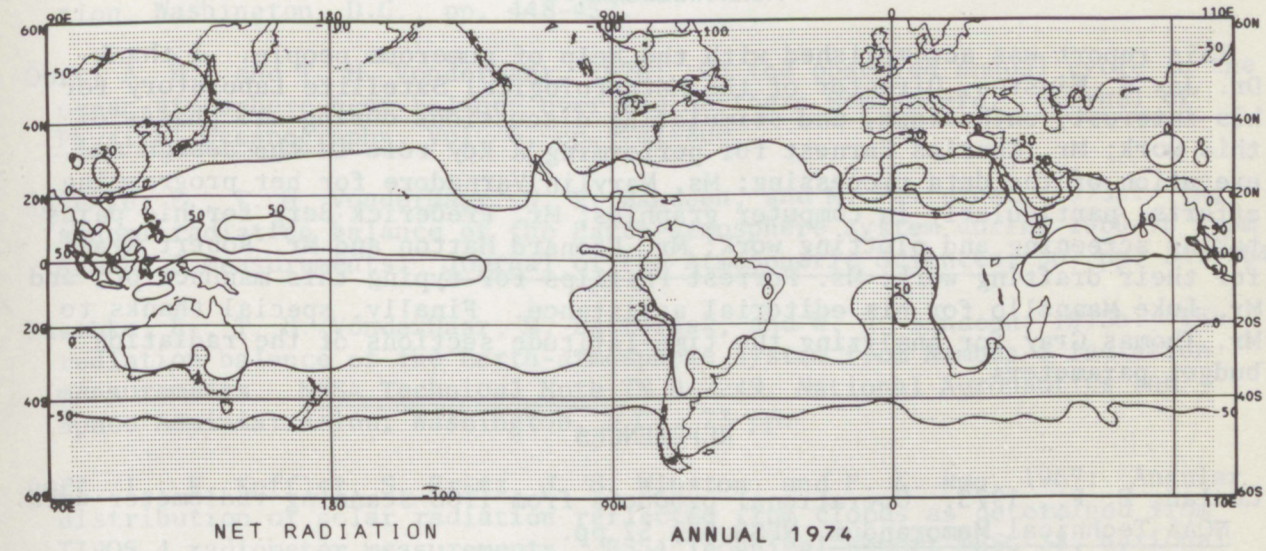

Figure 13.--Same as figure 10, except shows net radiation ($W \cdot m^{-2}$). Values less than zero are shaded.

albedo areas of the Sahara Desert and the low-level stratiform-type clouds found off the west coasts of North and South America and Africa. Those areas show relatively high albedos, greater than 40% in some instances, and also large outgoing longwave radiation because of their high temperatures. Because of this combination they exhibit net radiation deficits, as much as 50 $W \cdot m^{-2}$, in latitude zones which are otherwise regions of radiation surplus (fig. 13).

CONCLUDING REMARKS

Calculated values and some characteristics of the large-scale time-averaged state of the Earth-atmosphere radiation balance and its principal components have been presented. For the most part these results confirm some characteristics of earlier estimates of the radiation balance determined from satellite observations. Although differences were observed between the various estimates, it would be premature to place too much emphasis on them because, while all were based on satellite observations, they are by no means homogeneous with each other and each estimate was based on different instrumentation (mostly uncalibrated in space) and different sets of assumptions were applied to them. Finally, it should be pointed out that the observations from the NOAA series of satellites provide the opportunity to accumulate a fairly long continuous set of observations that are reasonably homogeneous with regard to spatial and sensor resolution as well as orbital characteristics. This set will be particularly useful for studying interannual variations on a variety of spatial scales ranging from the planetary to the regional, despite some of the simplifying assumptions used and difficulties encountered in deriving the radiational balance estimates. As indicated, more caution must be exercised when analyzing and interpreting individual grid points at high temporal resolution than when treating large-scale averages in space and time.

ACKNOWLEDGMENTS

This report was accomplished with the help of numerous people. I thank Dr. Jay S. Winston, Director of the Meteorological Satellite Laboratory for his interest, enthusiasm, and stimulating discussions during all phases of this work; Mr. Charles Earnest for performing a key role in the design and execution of the data processing; Ms. Marylin Varnadore for her programming efforts, particularly in computer graphics; Mr. Frederick Berg for his painstaking screening and plotting work; Mr. Leonard Hatton and Mr. Robert Ryan for their drafting work; Ms. Forrest Phillips for typing this manuscript; and Mr. Luke Mannello for his editorial assistance. Finally, special thanks to Mr. Thomas Gray for analyzing the time-latitude sections of the radiation budget parameters.

REFERENCES

Conlan, E. F., 1973: Operational products from ITOS scanning radiometer data. NOAA Technical Memorandum, NESS 52, 57 pp.

Ellis, R., and T. H. VonderHaar, 1976: The annual cycle in planetary radiation exchange with space. Proceedings of the Symposium on Meteorological Observations from Space: Their Contributions to the First GARP Global Experiment, the Nineteenth COSPAR Meeting, June 8-10, 1976, Philadelphia, Pa., pp. 280-282.

Gruber, A., 1972: Fluctuations in the position of the ITCZ in the Atlantic and Pacific Oceans. Journal of the Atmospheric Sciences, 29, pp. 193-197.

Gruber, A., 1976: Determination of the Earth-atmosphere radiation balance from NOAA satellites. Proceedings of the Symposium on Meteorological

Observations From Space: Their contribution to the First GARP Global Experiment, the nineteenth COSPAR Meeting, June 8-10, 1976, Philadelphia, Pa., pp. 265-269.

Jacobowitz, H., and A. Gruber, 1975: Calibration of the visible channel of the NOAA 2 scanning radiometer. Abstracts of Second Conference on Atmospheric Radiation, Arlington, Va., American Meteorological Society, Boston, Mass., p. 67.

Jacobowitz, H., W. L. Smith, H. B. Howell, and F. W. Nagle, 1977: The first eighteen months of planetary radiation budget measurements from the Nimbus 6 ERB experiment. In preparation.

Jones, G. D., 1973: Personal communication.

Jones, G. D., D. T. Hilleary, and B. Fredovich, 1965: A diffuse light source for calibrating meteorological satellite television cameras. Applied Optics, 4, pp. 307-309.

Leese, J., 1977: Personal communication.

List, R. J., 1958: Smithsonian Meteorological Tables, Smithsonian Institution, Washington, D.C., pp. 448-452.

Oort, A. H., and T. H. VonderHaar, 1976: On the observed annual cycle in the ocean-atmosphere heat balance over the Northern Hemisphere. Journal of Physical Oceanography, Vol. 6, pp. 781-800.

Raschke, E., T. H. VonderHaar, W. R. Bandeen, and M. Pasternak, 1973a: The annual radiation balance of the Earth-atmosphere system during 1969-70 from Nimbus 3 measurements. Journal of the Atmospheric Sciences, 30, pp. 341-364.

Raschke, E., T. H. VonderHaar, M. Pasternak, and W. R. Bandeen, 1973b: The radiation balance of the Earth-atmosphere system from Nimbus-3 radiation measurements. NASA Technical Note TN D-7249, National Aeronautics and Space Administration, Washington, D.C., 73 pp.

Ruff, I., R. Koffler, S. Fritz, J. S. Winston, and P. K. Rao, 1967: Angular distribution of solar radiation reflected from clouds as determined from TIROS 4 radiometer measurements. ESSA Technical Report NESC-38, National Environmental Satellite Center, Washington, D.C., 64 pp.

Schwalb, A., 1972: Modified version of improved TIROS operational satellite (ITOS D-G). NOAA Technical Memorandum NESS 35, National Environmental Satellite Service, Washington, D.C., 48 pp.

Schwalb, A., 1973: Personal communication.

Smith, W. L., J. Hickey, H. B. Howell, H. Jacobowitz, D. T. Hilleary, and A. J. Drummond, 1977: Nimbus 6 Earth radiation budget experiment. Applied Optics, 16, pp. 306-318.

Thekaekara, M. P., and A. J. Drummond, 1971: Standard values for the solar constant and its spectral components. Nature Physical Science, 229, pp. 6-9.

VonderHaar, T. H., and V. E. Suomi, 1971: Measurements of the Earth's radiation budget from satellites during a five-year period. Part 1: extended time and space means. Journal of the Atmospheric Sciences, 23, pp. 305-314.

Wark, D. Q., G. Yamamoto, and J. Lienesch, 1962: Infrared flux and surface temperature determinations from TIROS radiometer measurements. Meteorological Satellite Laboratory Report No. 10, U.S. Department of Commerce, Weather Bureau, Washington, D.C.

Winston, J. S., 1971: The annual course of zonal mean albedo as derived from ESSA 3 and 5 digitized picture data. Monthly Weather Review, 99, pp. 818-827.

Winston, J. S., 1976: Radiation budget variations (1975-76 compared with 1974-75). Proceedings of the NOAA Climate Diagnostics Workshop, Nov. 4-5, 1976, Washington, D.C., U.S. Department of Commerce.

Winston, J. S., and A. F. Krueger, 1977: Diagnosis of the satellite observed radiative heating in relation to the summer monsoon. Submitted to Pure and Applied Geophysics.

APPENDIX 1

In a strict sense the visible digital counts, because they are normalized, should be weighted by the cosine of the solar zenith angle before averaging. This in effect requires an average of un-normalized digital counts, which then has to be normalized by the average cosine of the solar zenith angle.

We can examine the possible error made by considering the averaging process. Let D be the normalized digital count and d be the un-normalized digital count. Then

$$D_i = di/CosZ_i \quad \text{and}$$

$$\overline{D} = \frac{1}{n}\sum_{i=1}^{n} (di/CosZ_i). \tag{1a}$$

The average formed from the un-normalized digital count divided by the average cosZ is

$$\overline{d} = (\frac{1}{n}\sum_{i=1}^{n} di)/(\frac{1}{n}\sum_{i=1}^{n} CosZ_i) \tag{2a}$$

$$= (\frac{1}{n}\sum_{i=1}^{n} di)/\overline{CosZ} .$$

The difference between $\overline{D}$ and $\overline{d}$ is

$$\overline{D} - \overline{d} = \frac{1}{n}\sum_{i=1}^{n} di\ (SecZ_i - \overline{SecZ}) \tag{3a}$$

or in terms of D_i the normalized digital count

$$\overline{D} - \overline{d} = \frac{1}{n}\sum_{i=1}^{n} D_i\,(\overline{CosZ} - CosZ_i)/\overline{CosZ}) . \tag{4a}$$

It is seen from eq (4a) that the magnitude of the error depends on the correlation between D_i and the percent deviation of the cosine of the solar zenith angle from its mean value over the averaging area $(\overline{CosZ} - CosZ_i)/\overline{CosZ}$. Since the data are generally uniformly distributed about some central point and since the averaging areas are fairly small (about 128 x 128 km), we can anticipate relatively homogeneous cloud conditions and small deviations from the mean value, $\overline{CosZ}$. Thus we anticipate only a small error introduced by our

averaging procedure. Given the orbital characteristics of the satellite a worst case estimate of the coefficient of D_i was attempted. The largest errors occur at low zenith angles near the polar night latitude. Under those circumstances the coefficient of D_i can be as high as 0.3. However, it should be anticipated that the average of all the values will be much less than that, since we do not expect a high correlation between D_i and $\frac{(\overline{CosZ} - CosZ_i)}{\overline{CosZ}}$.

APPENDIX 2

The NOAA 2 visible scanning radiometer is calibrated in luminance or brightness. Brightness is a measure of the light that the normal human eye would see. In the MKS system of units, it is given in lumens/steradian-m^2. However, for the NOAA 2 scanning radiometers, the level of brightness is expressed in foot-lamberts. A foot-lambert equals 3.426 lumens/steradian-m^2. The human eye has a frequency response that extends from about 4500 Å to 6500 Å and peaks at about 5500 Å (fig. 14). To obtain the total amount of energy corresponding to a given level of brightness, it is necessary to know what the "absolute luminous efficiency" is. This is defined as the ratio of the flux that is effectively sensed by the human eye to the flux that is intrinsic to the radiation. It is expressed mathematically as (List 1958):

$$K = K \max \frac{\int_0^\infty \overline{Y}_\lambda N_\lambda \, d_\lambda}{\int_0^\infty N_\lambda \, d_\lambda} \text{ (Lumens/Watt)} \qquad (1)$$

N_λ is the spectral radiance of the source - watts/sterad/area-wavelength of source

$\overline{Y}_\lambda$ is the relative spectral luminosity = $\frac{N_{\lambda m}}{N_\lambda}$

$N_{\lambda m}$ is the minimum amount of radiance to produce a given level of brightness.

Thus, $\overline{Y}_\lambda$ represents the ratio of the power at the wavelength of the eye's greatest sensitivity to produce a given brightness level to the power at the chosen wavelength necessary to produce the same brightness level.

K max = maximum attainable luminous efficiency and for a standard observer equals 680 lumens/Watt.

It is necessary to obtain a value for eq (1) to convert from luminance to radiance values. To accomplish this it is necessary to know the spectral radiance of the source. Information on the source used by the contractor is unfortunately quite scanty. According to A. Schwalb (1973) of NESS, the contractor used a source developed at NESS (Jones et al., 1965). Upon checking with Jones, I was able to obtain the spectral radiance of the source as reported in Jones et al., 1965. It was then possible to calculate a value for K from eq (1). The value obtained was 138.46 lumens/Watt or inversely 7.225×10^{-3} Watt/lumen. A foot-lambert equals 3.426 candles/m^2, which equals 3.426 lumens/steradian-m^2. Thus, multiplying calibrated values of foot-lamberts by 0.0248 ($7.225 \times 3.426 \times 10^{-3}$) provides a conversion from foot-lamberts to Watts/steradian-m^2.

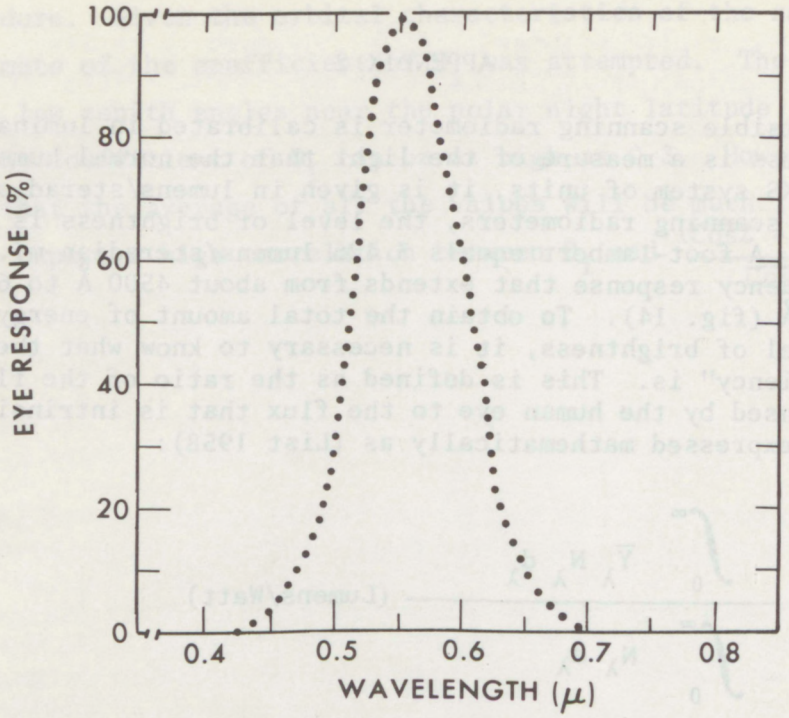

Figure 14.--Response of the human eye to visible radiation, based on the values adopted by the International Commission on Illumination. (Smithsonian Meteorological Table No. 149).

However, only 30.8% of the energy of the calibrating source* is in the spectral range of the radiometer (0.5μ to 0.9μ). Thus, the proper conversion factor is 0.0248 x 0.308 and is 7.64×10^{-3}. This conversion factor essentially takes into account the effect of two filters upon the calibrating source, one being the response of the normal human eye, and the other the response of the radiometer. The relationship between the two filters to the calibrating source is shown in figure 15. In calculating the conversion factor it was assumed that the source reported on by Jones et al. was the same as the one that the contractors used. If this was not the case, the results will be invalid. Schwalb (1973) has also indicated that independent calibration of the radiometers showed about a 15% variability, presumably for the same calibrating source. It is not clear what the cause of this variability was. In calculating the conversion factor, the operational calibration curve was used. For a perfectly diffuse reflector the reflexted flux is given by $\Pi \times 7.64 \times 10^{-3}$ and is 0.024. Thus multiplying foot-lamberts by 0.024 yields a measure of the reflected flux density in Watts/m^2, for a perfectly diffuse reflector.

To calculate reflectivity, it is necessary to obtain the filtered solar constant, i.e., the amount of solar energy contained in the spectral range of the radiometer. This was calculated to be 19.7% of the solar constant or

*Filtered by the response of the radiometer

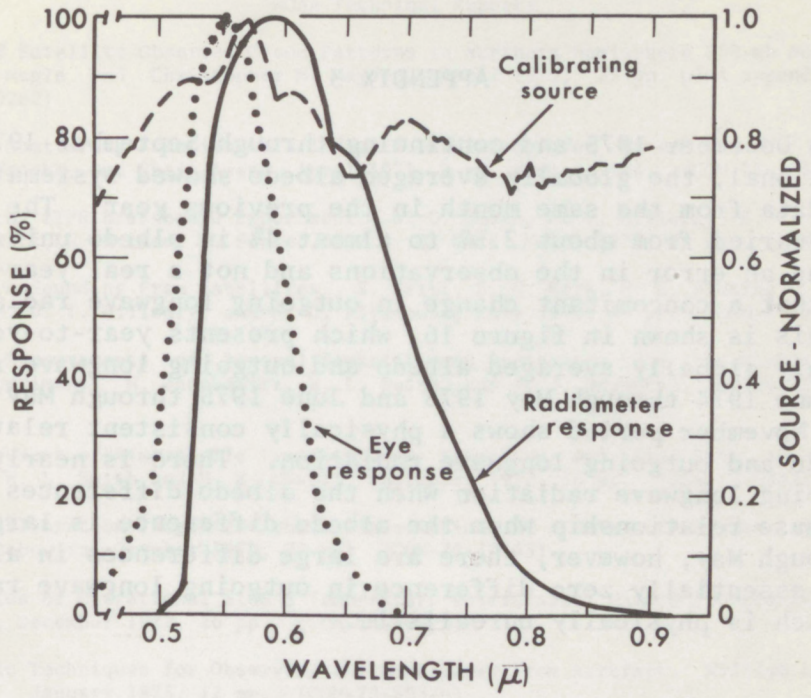

Figure 15.--Relationship between human eye response (dotted line), radiometer response (solid line), and calibrating source (dashed line). The calibrating source has been normalized; use ordinate on right side. Only the response of the F12 radiometer has been plotted. The other radiometer has a similar response.

1353 x 0.197 = 266.541 Watts/m^2. The reflected energy as measured by the satellite is archived in coded values of foot-lamberts. Each coded unit is worth 40 foot-lamberts. Thus a value of reflectivity R is given by the following:

$$R = \frac{40 \times D \times 0.024 \times 100}{266.541} = 0.3601D \text{ in } \%$$

D is the coded value of foot-lamberts and varies between 0 and 255 (Conlan 1973).

If it is assumed that the computed value of R is the same for the entire solar spectrum and that the value so computed is independent of solar zenith angle, then R is equal to the albedo of the Earth-atmosphere at the place of measurement.

APPENDIX 3

Starting in December 1975 and continuing through September 1976 when NOAA 5 became operational, the globally averaged albedo showed systematically lower values than data from the same month in the previous year. The magnitude of the decrease varied from about 2.5% to almost 4% in albedo units. The reason for suspecting an error in the observations and not a real year-to-year difference was that a concomitant change in outgoing longwave radiation was not observed. This is shown in figure 16, which presents year-to-year differences of mean monthly globally averaged albedo and outgoing longwave radiation for the period June 1974 through May 1975 and June 1975 through May 1976. The June through November period shows a physically consistent relationship between albedo and outgoing longwave radiation. There is nearly zero difference in outgoing longwave radiation when the albedo differences are small and and out-of-phase relationship when the albedo difference is large. From December through May, however, there are large differences in albedo between the 2 yr and essentially zero difference in outgoing longwave radiation, a condition which is physically unrealistic.

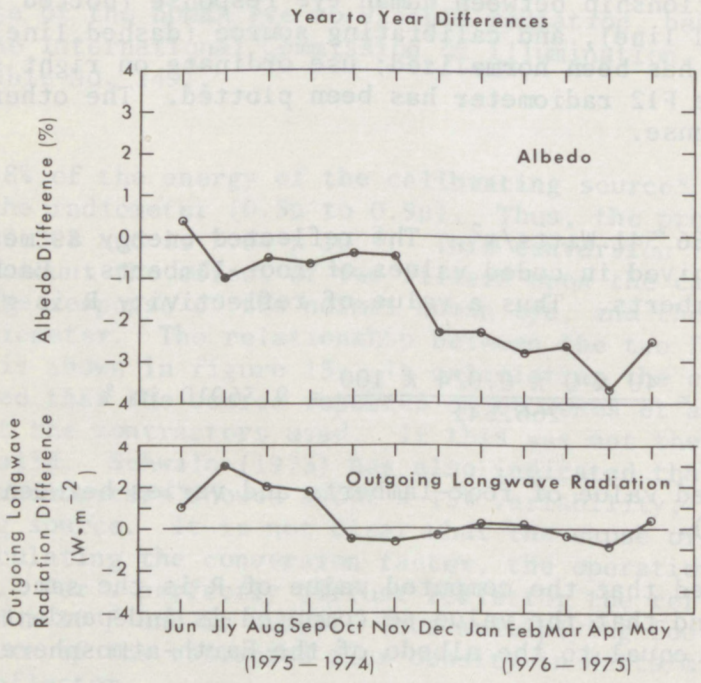

Figure 16.--Year-to-year differences, by month (1975-1974, 1976-1975), of albedo and outgoing longwave radiation.

(Continued from inside front cover)

NOAA Technical Reports

NESS 55 The Use of Satellite-Observed Cloud Patterns in Northern Hemisphere 500-mb Numerical Analysis. Roland E. Nagle and Christopher M. Hayden, April 1971, 25 pp. plus appendixes A, B, and C. (COM-73-50262)

NESS 57 Table of Scattering Function of Infrared Radiation for Water Clouds. Giichi Yamamoto, Masayuki Tanaka, and Shoji Asano, April 1971, 8 pp. plus tables. (COM-71-50312)

NESS 58 The Airborne ITPR Brassboard Experiment. W. L. Smith, D. T. Hilleary, E. C. Baldwin, W. Jacob, H. Jacobowitz, G. Nelson, S. Soules, and D. Q. Wark, March 1972, 74 pp. (COM-72-10557)

NESS 59 Temperature Sounding From Satellites. S. Fritz, D. Q. Wark, H. E. Fleming, W. L. Smith, H. Jacobowitz, D. T. Hilleary, and J. C. Alishouse, July 1972, 49 pp. (COM-72-50963)

NESS 60 Satellite Measurements of Aerosol Backscattered Radiation From the Nimbus F Earth Radiation Budget Experiment. H. Jacobowitz, W. L. Smith, and A. J. Drummond, August 1972, 9 pp. (COM-72-51031)

NESS 61 The Measurement of Atmospheric Transmittance From Sun and Sky With an Infrared Vertical Sounder. W. L. Smith and H. B. Howell, September 1972, 16 pp. (COM-73-50020)

NESS 62 Proposed Calibration Target for the Visible Channel of a Satellite Radiometer. K. L. Coulson and H. Jacobowitz, October 1972, 27 pp. (COM-73-10143)

NESS 63 Verification of Operational SIRS B Temperature Retrievals. Harold J. Brodrick and Christopher M. Hayden, December 1972, 26 pp. (COM-73-50279)

NESS 64 Radiometric Techniques for Observing the Atmosphere From Aircraft. William L. Smith and Warren J. Jacob, January 1973, 12 pp. (COM-73-50376)

NESS 65 Satellite Infrared Soundings From NOAA Spacecraft. L. M. McMillin, D. Q. Wark, J.M. Siomkajlo, P. G. Abel, A. Werbowetzki, L. A. Lauritson, J. A. Pritchard, D. S. Crosby, H. M. Woolf, R. C. Luebbe, M. P. Weinreb, H. E. Fleming, F. E. Bittner, and C. M. Hayden, September 1973, 112 pp. (COM-73-50936/6AS)

NESS 66 Effects of Aerosols on the Determination of the Temperature of the Earth's Surface From Radiance Measurements at 11.2 m. H. Jacobowitz and K. L. Coulson, September 1973, 18 pp. (COM-74-50013)

NESS 67 Vertical Resolution of Temperature Profiles for High Resolution Infrared Radiation Sounder (HIRS). Y. M. Chen, H. M. Woolf, and W. L. Smith, January 1974, 14 pp. (COM-74-50230)

NESS 68 Dependence of Antenna Temperature on the Polarization of Emitted Radiation for a Scanning Microwave Radiometer. Norman C. Grody, January 1974, 11 pp. (COM-74-50431/AS)

NESS 69 An Evaluation of May 1971 Satellite-Derived Sea Surface Temperatures for the Southern Hemisphere. P. Krishna Rao, April 1974, 13 pp. (COM-74-50643/AS)

NESS 70 Compatibility of Low-Cloud Vectors and Rawins for Synoptic Scale Analysis. L. F. Hubert and L. F. Whitney, Jr., October 1974, 26 pp. (COM-75-50065/AS)

NESS 71 An Intercomparison of Meteorological Parameters Derived From Radiosonde and Satellite Vertical Temperature Cross Sections. W. L. Smith and H. M. Woolf, November 1974, 13 pp. (COM-75-10432/AS)

NESS 72 An Intercomparison of Radiosonde and Satellite-Derived Cross Sections During the AMTEX. W. C. Shen, W. L. Smith, and H. M. Woolf, February 1975, 18 pp. (COM-75-10439/AS)

NESS 73 Evaluation of a Balanced 300-mb Height Analysis as a Reference Level for Satellite-Derived soundings. Albert Thomasell, Jr., December 1975, 25 pp. (PB-253-058)

NESS 74 On the Estimation of Areal Windspeed Distribution in Tropical Cyclones With the Use of Satellite Data. Andrew Timchalk, August 1976, 41 pp. (PB-261-971)

NESS 75 Guide for Designing RF Ground Receiving Stations for TIROS-N. John R. Schneider, December 1976, 126 pp. (PB-262-931)